2016-01-04

Field observation of low-to-mid-frequency acoustic propagation characteristics of an estuarine salt wedge

Reeder, D. Benjamin

J. Acoust. Soc. Am. 139 (1) (January 2016), p. 21-29
http://hdl.handle.net/10945/48436

Field observation of low-to-mid-frequency acoustic propagation characteristics of an estuarine salt wedge

D. Benjamin Reeder[a)]
Department of Oceanography, Naval Postgraduate School, 833 Dyer Road, Monterey, California 93943, USA

(Received 21 April 2015; revised 18 September 2015; accepted 8 December 2015; published online 4 January 2016)

The estuarine environment often hosts a salt wedge, the stratification of which is a function of the tide's range and speed of advance, river discharge volumetric flow rate, and river mouth morphology. Competing effects of temperature and salinity on sound speed in this stratified environment control the degree of acoustic refraction occurring along an acoustic path. A field experiment was carried out in the Columbia River Estuary to test the hypothesis: the estuarine salt wedge is acoustically observable in terms of low-to-mid-frequency acoustic propagation. Linear frequency-modulated acoustic signals in the 500–2000 Hz band were transmitted during the advance and retreat of the salt wedge during May 27–29, 2013. Results demonstrate that the salt wedge front is the dominant physical mechanism controlling acoustic propagation in this environment: received signal energy is relatively stable before and after the passage of the salt wedge front when the acoustic path consists of a single medium (either entirely fresh water or entirely salt water), and suffers a 10–15 dB loss and increased variability during salt wedge front passage. Physical parameters and acoustic propagation modeling corroborate and inform the acoustic observations.
[http://dx.doi.org/10.1121/1.4939108]

[TFD] Pages: 21–29

I. INTRODUCTION

The estuarine environment often hosts a salt wedge—denser seawater advected by the rising tide under fresh water discharged by the river. The nature of the stratification is a function of the tide's range and speed of advance, river discharge volumetric flow rate, and river mouth morphology (Dyer, 1998). When the fresh water is warm relative to the salt water, the competing effects of temperature and salinity on sound speed may create a sound speed gradient too small to cause acoustic refraction. When the fresh water is cold relative to the salt water, both temperature and salinity will contribute to create a stronger sound speed gradient compared to that observed during summer. Acoustically, this environment consists of two isospeed layers separated by a thin, range- and depth-dependent, high-gradient layer comprising the salt wedge front. While this three-layer, very shallow water acoustic waveguide is typically dominated by high-angle multipath propagation, refraction occurring in the gradient layer has the potential to facilitate the ducting of low-angle energy in the upper layer and the creation of a shadow zone in the lower layer. Additionally, the statistical variability of TL is expected to increase due to the spatiotemporal dynamics of the salt wedge structure as it advances and retreats on the rising and falling tides.

Beyond these physics-based expectations of phenomenology, relatively few acoustical studies have been carried out in rivers, estuaries, or other energetic environments; nearly all acoustical work in such environments has been done at higher frequencies, in the 10's and 100's of kHz. Those few studies carried out in confined coastal and inland waterways that are found in the literature have focused on a variety of issues, including acoustic scintillation to estimate current flow (Di Iorio and Farmer, 1994), active sonar systems for biological stock assessment and fisheries management (Xie, 2000), homeland security applications (Stolkin *et al.*, 2006), acoustical communication (van Walree *et al.*, 2007), acoustical monitoring of tidal bores (Zhu *et al.*, 2010), marine mammal surveys (Dong *et al.*, 2011), seasonal trends in a large remote fjord (McConnell *et al.*, 1992), recreational boat noise in waterways (Haviland-Howell *et al.*, 2007), ambient noise in freshwater habitats (Wysocki *et al.*, 2007), high-frequency noise spectra in shallow brackish water (Poikonen, 2010), long-term noise trends in large, industrialized rivers (Vracar and Mijic, 2011), acoustical monitoring of ship traffic (Fillinger *et al.*, 2011), acoustic attenuation properties in a river (Roh *et al.*, 2008), site-specific acoustic propagation models for the lower Hudson River Estuary (Radhakrishnan, 2009), and acoustic quantification of stratified turbulence in the Connecticut River (Lavery *et al.*, 2013).

Investigations of near-shore and in-shore environments have, rightly, focused on geological, thermodynamic, and hydrodynamic parameters of the estuarine/riverine environment, such as depth, width, bottom composition and morphology, water temperature and salinity structure, tides, current profiles, turbulence, and sediment transport. A complementary acoustical characterization of the estuarine/riverine environment provides another layer of information to facilitate a more complete understanding of the physical environment.

To this end, a small acoustical field experiment was carried out in the Mouth of the Columbia River (MCR) within

a)Electronic mail: dbreeder@nps.edu

the context of a larger hydrodynamic field experiment entitled Rivers and Inlets II (RIVET II) funded by the Office of Naval Research. The acoustical portion of RIVET II was carried out during the second half of May, 2013 aboard the R/V Oceanus, operated by Oregon State University (OSU). The objective was to characterize the acoustical environment at MCR, in terms of ambient noise field statistics and acoustic propagation characteristics. This paper focuses on acoustic propagation characteristics of 500–2000 Hz linear frequency-modulated (LFM) signals to test the hypothesis: the estuarine salt wedge is acoustically observable at low-to-mid frequencies.

The paper is organized as follows. Section II presents information on the oceanographic environment and the *in situ* data collected, Sec. III provides observations from the data analysis, Sec. IV includes acoustic propagation modeling results, Sec. V contains discussion, and Sec. VI presents conclusions.

II. ENVIRONMENTAL SETTING AND DATA COLLECTION

The Columbia River is one of the major rivers of North America; as the largest river on the west coast of the United States, it drains a vast watershed of western North America, approximately 669 000 km^2 in area (Elias *et al*., 2012). The estuary is classified as partially mixed (Neal, 1972) and mesotidal (Sherwood and Creager, 1990), possessing mixed diurnal and semidiurnal tides with a mean range of approximately 2 m (Neal, 1972) and maximum observed ranges as great as 3.4 m during spring tides (Gelfenbaum, 1983). The degree of stratification varies from weak (well-mixed) to highly stratified with a salt wedge, depending on tidal excursion and river flow. The overall surface area and outflow of the estuary is markedly diminished relative to historical values and highly regulated by numerous dams constructed upriver for irrigation, flood control, and hydropower generation; however, the estuary remains a highly energetic environment having strong tidal currents and large river volumetric flow rates, the variability of which can be described by three "seasons" possessing differing flows. The fall season (August to November) is characterized by the lowest flows. The winter season also has generally low flows, punctuated by short periods of high flows due to precipitation from winter storms. This field experiment was carried out during the spring, when river flows are the highest (Sherwood and Creager, 1990). River flow at the mouth has an annual average of approximately 7300 m^3/s and varies from an average summer-fall low of 2500 m^3/s to a spring freshet of about 11 000 m^3/s, when associated peak tidal surface velocities are typically 2.6 m/s and often exceed 3 m/s during ebb tide. Very rough surface conditions can be produced via wave-current interaction by predominantly westerly winds and ocean swells during ebb tides: significant wave height averages 1.2 m during summer, but averages 3 m in winter, and can exceed 14 m during heavy winter storms (Elias *et al*., 2012).

The asymmetrical ebb-tidal delta extends 7 km east of the river mouth and 15 km along the coast. Average annual sediment discharge by the Columbia River is about 7.6×10^6 metric tons, which is lower than historical values prior to dam construction, indicating that a significant amount of sediment remains trapped in upstream man-made reservoirs. Most of the sediment transported to the river mouth consists of locally sourced sand from adjacent bays, tributaries and the estuarine shoreline. Bottom sediment is predominantly fine sand with a mean grain size of 2.75ϕ (0.149 mm) (Sherwood and Creager, 1990). The river is dredged continuously spring through fall each year to maintain a 17 m deep navigational channel for the safe passage of commercial ships transporting cargo upriver to several major ports (Sherwood *et al*., 1990; Elias *et al*., 2012). Due to high flow rates and available sediment, bedforms having amplitudes between 0.7 and 2.1 m and wavelengths between 20 and 90 m have been observed in various places in MCR (Gelfenbaum *et al*., 2014).

The experimental area spanned from several kilometers west of the North Jetty and South Jetty at the river mouth to points just west of the A-M bridge in the North Channel (Fig. 1). During flood and ebb, the salt wedge advances and retreats through the river mouth. Figure 2 shows the surface expression of the salt wedge front on May 27 during flood near high tide. The picture was taken from the ship at Station S2, looking east toward Jetty A at the southern tip of Cape Disappointment. It can be seen in the figure that the salt wedge is a very three-dimensional feature: the deep shipping channel depicted in the navigation chart in Fig. 1 appears to "channel" the denser water of the salt wedge into the center of the estuary, creating a semi-circular salt wedge front surface expression. Well before the tide reverses, the less-dense river water makes its way around the north and south sides of the salt wedge front surface expression, creating a thin fresh water layer above the salt water. The convergence of the advancing ocean tide against the strong river outflow generates highly dynamic circulation and turbulence (Jay and Smith, 1990). This turbulent convergence of the two water masses is evident in Fig. 3 showing the salt wedge front surface expression, which is characterized by confused, breaking waves (Thomson *et al*., 2014). There is also significant downwelling at the front, enhancing bubble subduction, which has a potential impact on acoustic propagation.

Hydrophones, temperature and pressure sensors, and acoustic current meters were moored at multiple locations throughout the experimental area. CTD casts were conducted throughout the experiment, the data from which were provided to the Center for Coastal Margin Observation and Prediction (CMOP) in Portland, OR for validation of their river forecast model, predictions from which were used as environmental input to acoustic propagation modeling (discussed in Sec. IV).

During a procession and a recession of the salt wedge during May 27–29, 2013, acoustic signals were transmitted from an acoustic source deployed over the side of the ship at Station S2 and observed by a hydrophone mounted on a tripod 1 m above the riverbed at Station A5 (Fig. 1). The surface condition during both periods consisted of locally generated wind waves and ocean swell entering the estuary from the southwest. This 1.36 km long acoustic transect,

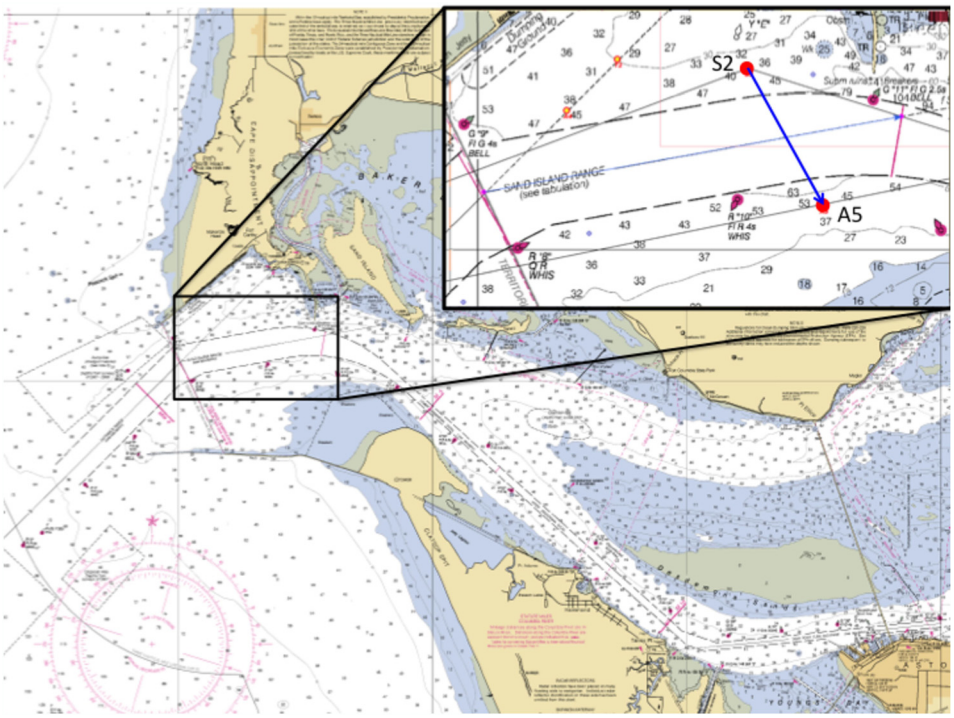

FIG. 1. (Color online) Mouth of the Columbia River: Inset shows Station S2 where the acoustic source was deployed over the side of the ship, and Station A5 where the receiver was deployed on a tripod 1 m above the riverbed. The acoustic transect was 1.36 km long. Note the asymmetry of the estuary.

transverse to the direction of salt wedge movement, was strategically chosen to provide the optimal geometry to observe the refractive properties of the salt wedge. The 2-s long, linear frequency-modulated (LFM) acoustic signals were transmitted in the 500–2000 Hz band once every 10 s and received at the hydrophone using a sampling frequency of 27.33 kHz. The received signals are match-filtered in the frequency domain. The matched-filter approach increases temporal resolution, improves SNR, acts as an in-band noise filter, and results in the multipath arrival structure of the compressed pulse (i.e., pulse response), measured as a function of time. The sound energy level (SEL) is defined as

$$SEL = 10\log\left(\int_0^T p^2(t)dt\right)\text{dB re 1 }\mu\text{Pa}^2 - \text{s}, \quad (1)$$

where $p(t)$ is the matched-filter output and T is the integration period equal to 0.5 s. The results presented here focus on data from one flood and one ebb during this period.

III. OBSERVATIONS

A. Ebb

Figure 4 presents data collected during ebb on May 28–29. The top panel shows sound speed as a function of depth (m) and range (m) along the acoustic path between the source at Station S2 and the receiver at Station A5. This across-channel transect is shown looking from west to east into the estuary as the salt wedge recedes from the estuary. Using the Chen-Millero equation, the sound speed is converted from temperature and salinity profiles provided by

FIG. 2. (Color online) Surface expression of the salt wedge front on May 27 during flood near high tide. The picture was taken from the ship at Station S2, looking east toward Jetty A at the southern tip of Cape Disappointment.

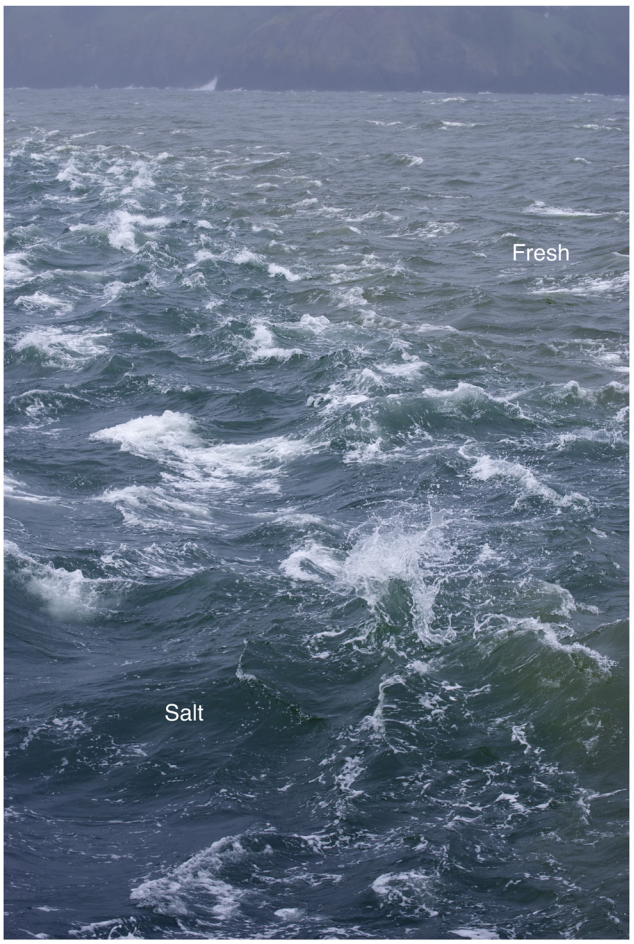

FIG. 3. (Color online) The turbulent convergence of the advancing ocean tide against the strong river outflow is evident in the salt wedge front surface expression, characterized by confused, breaking waves and downwelling of the salt water under the fresh river water.

CMOP (Chen and Millero, 1977). The source is depicted on the left at 4 m water depth and the receiver is depicted on the right 1 m above the riverbed. The CMOP model output was provided in 36 s increments, and this particular profile is the one for 0245Z on May 29, which is the approximate time at which the acoustic source occupies the depth of greatest sound speed gradient. The bathymetry is based upon United States Geological Survey (USGS) multi-beam echosounder bathymetric surveys conducted in 2012 and provided by CMOP. In this particular profile, depth varies from 16 m at Station S2 to a maximum of 27 m in the center of the channel, back up to 17 m at Station A5; modeled sound speed varies from a minimum of 1476 m/s on the southern side of the transect near the surface above the receiver at Station A5 to a maximum sound speed of 1490 m/s near the riverbed in the northern portion of the navigation channel.

The middle panel shows sound speed (m/s) as a function of depth (m) from CTD profiles collected on a Castaway CTD hand-deployed over the side of the ship in approximately 15-min intervals during the 6-h acoustic transmission period from 2300Z on May 28 to 0500Z on May 29. Sound speed is observed to vary between 1460 and 1490 m/s primarily due to the salinity variation of 28 psu, while temperature varied by only 1.5 °C. Note that as the salt wedge recedes during ebb, 0245Z is the approximate time at which the source at 4 m water depth moves from salt water to fresh water.

The bottom panel shows 1-min averaged relative signal energy level (SEL) in dB re 1 μPa^2−s (normalized to the maximum SEL during the 6-h observation period) observed at Station A5 vs time on the same scale as shown in the middle panel. SEL is relatively stable prior to 0100Z, decreases 10 dB during a 1[1/2] hour period, reaches a minimum at ∼0230Z, then rapidly increases 10 dB during a 45 min period, finally returning at 0315Z to approximately the same level as observed prior to 0100Z. Except for the large, anomalous nulls occurring at ∼0125Z and ∼0150Z during the 1[1/2] hour period of decreasing SEL, the SEL variability remains relatively constant throughout the 6-h period. The sound speed gradient during ebb, while significant, is weaker than during flood, as discussed in Sec. IV.

B. Flood

Figure 5 follows the same structure as Fig. 4 but presents results for flood on May 27. The top panel shows sound speed for the same acoustic transect between Stations S2 and A5, with the acoustic source deployed at 7 m water depth and the receiver in the same location 1 m above the riverbed. The CMOP model output timestamp is 1915Z in this case, which is the approximate time at which the acoustic source occupies the depth of greatest sound speed gradient. Modeled sound speed varies from a minimum of 1460 m/s in the near-surface waters across the entire transect to a maximum sound speed of 1490 m/s in the lower portion of the water column across the northern portion of the navigation channel. This asymmetry in sound speed across the acoustic transect (in both ebb and flood) reflects the geographical asymmetry of the navigation channel mentioned in Sec. II and shown in Fig. 1.

The middle panel again shows sound speed (m/s) as a function of depth (m) computed from the Castaway CTD deployed over the side of the ship in approximately 15-min intervals during the 6-h acoustic transmission period from 1530Z to 2130Z on May 27. Sound speed is observed to vary between 1460 and 1490 m/s primarily due to the salinity variation of 28 psu, while temperature varied by only 1.5 °C. Note that as the salt wedge advances during flood, 1925Z is the approximate time at which the source at 7 m water depth moves from fresh water to salt water.

The bottom panel shows relatively stable SEL prior to 1700Z; SEL then slowly decreases approximately 15 dB during a 2[1/2] hour period, reaches a minimum at approximately 1925Z, then rapidly increases 15 dB during a 1 h period, finally returning at 2030Z to approximately the same level as observed prior to 1700Z. SEL variability during the period of decreasing and increasing SEL (∼1730Z–2030Z) is greater than the variability at the beginning and end of the transmission period.

IV. ACOUSTIC MODELING

In order to provide insight into the physics of the acoustic propagation through the salt wedge, the 2D Bellhop

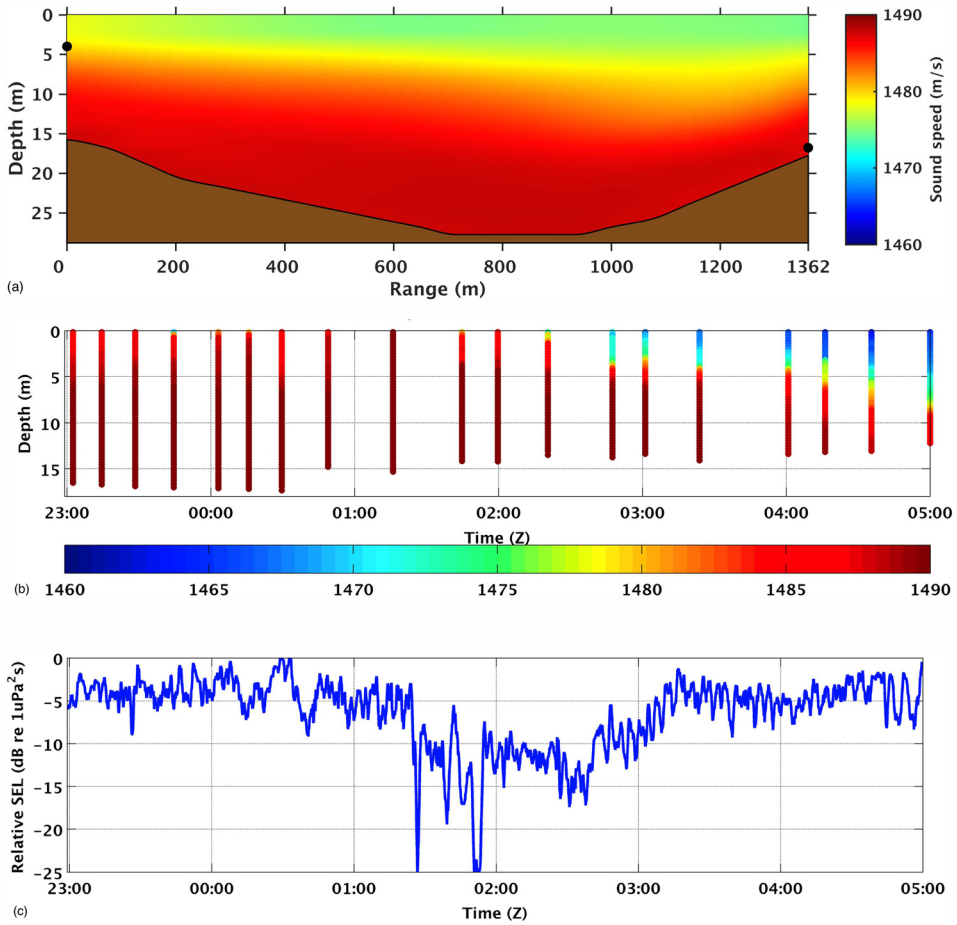

FIG. 4. (Color online) (a) Modeled sound speed (m/s) vs depth (m) and range (m) along the S2-A5 acoustic transect at model time 0245Z on May 29, 2013. This across-channel transect is shown looking from west to east into the estuary. The solid circle on the left marks the position of the acoustic source 4 m below the surface. The solid circle on the right marks the position of the acoustic receiver mounted on a tripod 1 m above the riverbed at Station A5. (*Modeled sound speed courtesy of CMOP.*) (b) Sound speed (m/s) vs depth (m) and time (Z) at Station S2 based on multiple CTD casts during the 6 h period of the acoustic transmissions shown in the lower panel. (c) Relative signal energy level (dB re 1 μPa^2 s) vs time (Z) observed at Station A5 on May 28–29.

coherent Gaussian beam acoustic propagation model (Porter and Bucker, 1987) was employed to compute band-averaged TL between the source at Station S2 and the receiver at Station A5 for the entire acoustic transmission period during flood on May 27. In the cross-range direction, the bathymetry was modeled as planar. In the along-path direction, the environment was modeled as range-dependent in terms of water column sound speed and bathymetric depth, and range-independent in terms of the geoacoustic parameters of the seabed and a planar sea surface. Range-dependent sound speed and bathymetry were derived from the CMOP profiles of temperature and salinity. The geoacoustic parameters associated with the predominantly fine sandy sediment with mean grain size of 2.75ϕ (0.149 mm) were a sound speed (c) of 1620 m/s, density (ρ) of 1.83 g/cm^3, and attenuation (α) of 0.365 dB/m (Sherwood and Creager, 1990; Zhou *et al.*, 2009). An omnidirectional point source was modeled to represent the source used during the field experiment.

Figure 6 shows the same observed relative SEL during flood on May 27 as shown in Fig. 5. The thicker solid line represents acoustic propagation modeling results in terms of modeled SEL received at the hydrophone at Station A5 based on CMOP temperature and salinity profiles in 360-s increments, computed every 5 Hz at a spatial resolution of [1/4] acoustic wavelength, and averaged across the 500–2000 Hz band. While appearing straight-forward, it is worth noting that this model result required 36 421 model runs, each of which consumed 1–4 CPU hours, totaling approximately 100 000 CPU hours. The modeled SEL shows a similar trend as the data: A relatively stable SEL prior to 1700Z, a slow decrease during a 2[1/2] hour period reaching a minimum at approximately 1920Z, followed by an increase over a 1 h period to approximately the same level as observed prior to 1700Z. While showing similar trends, the modeled SEL decreases by only 6–8 dB, significantly less than the 15 dB decrease observed in the data.

V. DISCUSSION

Before the entrance of the salt wedge during flood (Fig. 5), the acoustic transect is composed of nearly isospeed fresh water which supports the SEL observed prior to 1700Z. As the salt wedge front crosses the acoustic transect along the riverbed, the higher speed water in the salt wedge causes a slowly increasing amount of the acoustic energy to be refracted up and away from the receiver at Station A5, with some energy being trapped in the thin near-surface fresh water layer above the salt wedge (Reeder, 2013). When the salt wedge front passes the acoustic source at ~1915–1930Z, the strong sound speed gradient in which the acoustic source is located causes the greatest degree of acoustic refraction of the entire period, resulting in the lowest observed SEL at Station A5. As the source enters the salt wedge and the acoustic transect is increasingly composed of salt water, the SEL observed at A5 rapidly increases and finally attains its pre-salt wedge passage level. A nearly identical process occurs during ebb tide as the salt wedge recedes, as seen in Fig. 4, but the stratification is weaker during ebb than flood. The weaker

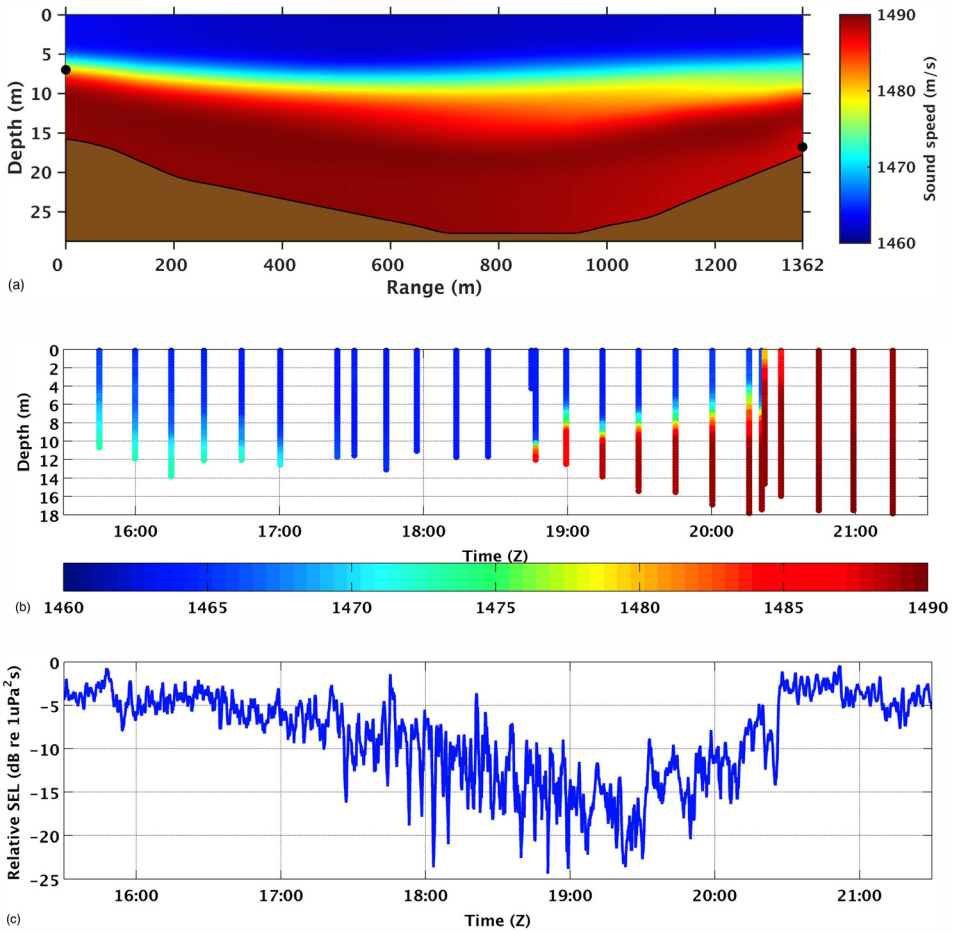

FIG. 5. (Color online) (a) Modeled sound speed (m/s) vs depth (m) and range (m) along the S2-A5 acoustic transect at model time 1915Z on May 27, 2013. The solid circle on the left marks the position of the acoustic source 7 m below the surface. The solid circle on the right marks the position of the acoustic receiver mounted on a tripod 1 m above the riverbed at Station A5. (*Modeled sound speed courtesy of CMOP*.) (b) Sound speed (m/s) vs depth (m) and time (Z) at Station S2 based on multiple CTD casts during the 6 h period of the acoustic transmissions shown in the lower panel. (c) Relative signal energy level (dB re 1 μPa^2 s) vs time (Z) observed at Station A5 on May 27.

sound speed gradient causes weaker upward refraction, resulting in a smaller decrease of 10 dB in SEL observed at Station A5.

The acoustic propagation modeling supports this interpretation; however, modeled SEL decreases by less than that observed in the data. Differences between modeled and observed SEL are likely due to several potential factors: (1) As mentioned earlier, the salt wedge front is a very three-dimensional feature, so the higher-speed water of the salt wedge not only refracts the acoustic energy up and away from the receiver at Station A5, but also refracts the energy out of plane and to the left (upriver) as the salt wedge front occupies the acoustic transect. Additionally, the riverbed slopes to the east between Station S2 and Station A5. Acoustic energy interacting with the sloping riverbed will be reflected out of plane to the east (regardless of the presence or absence of the salt wedge). This 3D acoustic propagation consisting of horizontal refraction by the water column and horizontal reflection by the riverbed is not accounted for in the 2D acoustic model. (2) The Gaussian beam model is not a full-physics model and does not properly represent all propagation loss mechanisms, such as diffraction and geometrical dispersion (Etter, 2003), resulting in an underprediction of TL. (3) The acoustic modeling is dependent upon how accurately the environmental input represents the actual conditions. It has been observed in other studies (Geyer, 2014) that the observed salinity gradients *in situ* at MCR are greater than what are represented by the modeled salinity profiles. The weaker-than-actual gradients in the environmental input to the acoustic model result in an underprediction of the degree of refraction that is actually occurring. (4) The accuracy of the geoacoustic parameters used to represent the riverbed is important. If the modeled parameters represent a riverbed that is less lossy than actual, the model will underpredict higher-angle energy loss and, consequently, the amount of SEL decrease during salt wedge

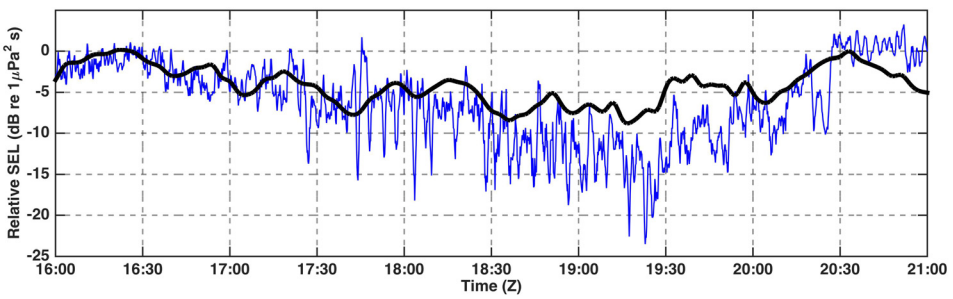

FIG. 6. (Color online) Modeled SEL (dB re 1 μPa^2 s) received at the hydrophone 1 m above the riverbed at Station A5 for each of the CMOP profiles in 360-s increments during flood on May 27, and observed SEL (thinner line) during the same period [identical to Fig. 5(c)].

passage. (5) The sea surface condition was modeled as planar, which is inconsistent with actual conditions; the very localized, roughened sea surface associated with the passage of the salt wedge front causes acoustic scattering and diminishes the coherence of the observed signal, resulting in an observed SEL lower than modeled with a planar sea surface.

In addition to overall levels and trends of received signal energy, another phenomenon of interest is the increased SEL variability during the period when the salt wedge front occupies the acoustic transect. Potential mechanisms contributing to this variability include: (1) While the sound speed was not sampled along the acoustic transect during the

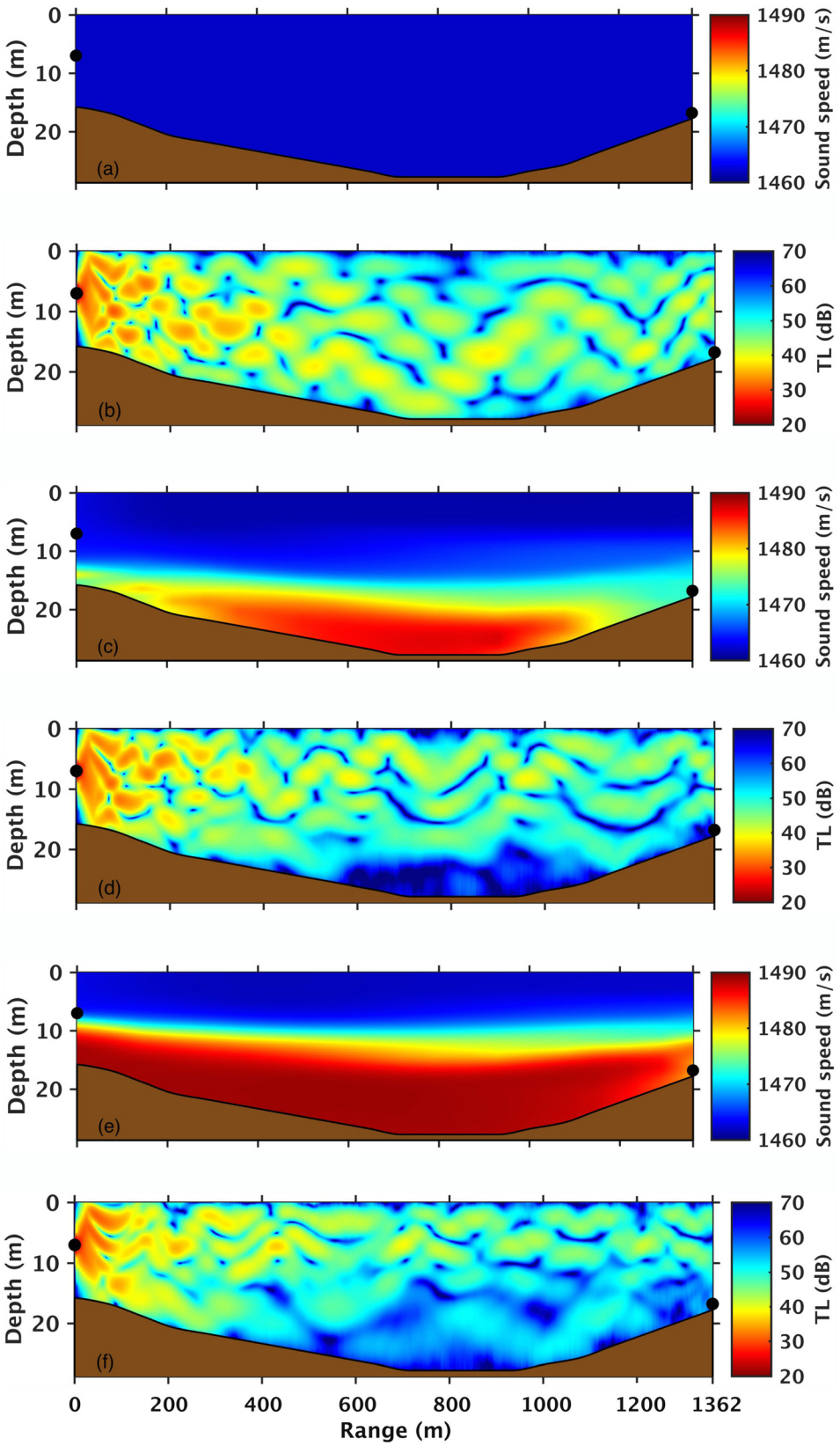

FIG. 7. (Color online) Sound speed (m/s) and associated predicted TL (dB re 1 μPa^2 s) as a function of depth (m) and range (m) for three waveguide conditions: (1) before the entrance of the salt wedge with an unstratified, isospeed (1462 m/s) waveguide [(a), (b)]; (2) during the advance of the salt wedge on the rising tide with a 12–15 m thick freshwater layer above the seawater [(c), (d)]; and (3) later in the tidal cycle with a 7–9 m thick freshwater layer above the seawater [(e), (f)]. The TL is computed for a 1250 Hz source at 7 water depth, using the same environmental parameters employed for Fig. 6.

transmission period, it is reasonable to expect that the turbulent convergence of the advancing ocean tide against the strong river outflow and the subsequent overturning and mixing increases the variability of the sound speed structure, resulting in increased variability in the observed SEL. (2) Internal waves have been observed to propagate on top of the salt wedge (McNeil *et al*., 2012), which is another source of sound speed structure perturbation that would further increase the variability of the observed SEL. (3) Dynamic surface conditions over the course of the observation period, as well as acoustic scattering and absorption by subducted bubbles from breaking waves and downwelling at the salt wedge front surface expression seen in Figs. 2 and 3 could contribute to the variability. (4) As mentioned earlier, bedforms have been observed in the estuary; in fact, the largest bedforms observed in 2013 are located immediately east (upstream) of the acoustic transect. Bedform-induced oscillations in the ebb current would contribute to fluctuations in the sound speed structure, resulting in increased variability in the observed SEL. (5) Significant populations of fish of various species occupy and transit through MCR. Fish, particularly those with swimbladders, scatter and absorb sound in the frequency band used in this field experiment (Diachok, 1999; Reeder and Stanton, 2004). The presence of fish schools of dynamic sizes and shapes would certainly contribute to a reduction in observed SEL as well as variability. Each of these mechanisms requires further investigation.

The preceding discussion is focused on acoustic energy observed at the receiver near the riverbed. While not directly observed in this field experiment, acoustic modeling demonstrates that some of the acoustic energy refracted upward by the salt wedge is trapped in the fresh water surface duct above the salt wedge. To illustrate this mechanism and to support the interpretation of the propagation mechanisms discussed earlier, Fig. 7 shows sound speed (m/s) and associated predicted TL (dB re 1 μPa^2 s) as a function of depth (m) and range (m) for three waveguide conditions: (1) before the entrance of the salt wedge with an unstratified, isospeed (1462 m/s) waveguide [(a), (b)], (2) during the advance of the salt wedge on the rising tide with a 12–15 m thick freshwater layer above the seawater [(c), (d)], and (3) later in the tidal cycle with a 7–9 m thick freshwater layer above the seawater [(e), (f)]]. The TL is computed for a 1250 Hz source at 7 water depth, using the same environmental parameters employed for Fig. 6. The isospeed waveguide in Fig. 7(a) supports the acoustic field seen in Fig. 7(b) containing only geometrical spreading and scattering, and no refraction. As the salt wedge advances into the estuary, the stratified waveguide in Fig. 7(c) begins to refract some of the acoustic energy up and away from the riverbed in the center of the channel. By the time the stratification approaches the depth of the source later in the flood tide as shown in Fig. 7(e), the surface duct is thinner yet traps a significant portion of the acoustic energy above the salt wedge as seen in Fig. 7(f). Once the salt wedge advances to the point where salt water fills the water column along the entire acoustic transect, the waveguide returns to isospeed conditions and the acoustic field returns to what is seen in Fig. 7(b).

Further acoustic modeling (not shown here) demonstrates that this acoustic ducting in the near-surface fresh water layer is time and frequency dependent: as the salt wedge advances on the flood, lower frequency energy is initially trapped but then progressively escapes as the surface duct thins with the advancing tide. In terms of SEL vs time, the slow decrease over the two hour period between 1700Z and 1930Z in Fig. 5(a) is initially partially due to ducting of lower frequency energy, followed by ducting at progressively higher frequencies; by the end of the period at high tide when the acoustic transect is composed completely of salt water, there is no longer a surface duct (nor vertical or horizontal refraction), causing the SEL to reach approximately the same level as observed before the entrance of the salt wedge. Future investigations will include 3D acoustic propagation modeling and modal analysis of this layered waveguide.

VI. CONCLUSIONS

A field experiment was carried out in the Columbia River Estuary during May 27–29, 2013 to acoustically observe the propagation characteristics of the estuarine salt wedge. During one flood and one ebb, linear frequency-modulated (LFM) acoustic signals in the 500–2000 Hz band were transmitted by an acoustic source deployed over the side of the ship at Station S2 and observed by a hydrophone 1.36 km distant at Station A5.

Observations and associated acoustic modeling results demonstrate that the salt wedge front is the dominant physical mechanism controlling acoustic propagation in this environment: received signal energy is relatively stable before and after the passage of the salt wedge front when the acoustic path consists of a single medium (either entirely fresh water or entirely salt water), and suffers a 10–15 dB loss and increased variability in a dual-media environment during salt wedge front passage due to vertical and horizontal refraction of energy up and out-of-plane from the receiver. Phenomenologically, acoustic propagation characteristics of the estuarine environment, in terms of average energy level and variance, will depend upon the position of the source and receiver relative to the salt wedge, acoustic frequency and environmental parameters, including the three-dimensional salt wedge-induced sound speed gradient, riverbed sediment acoustic properties and morphology (e.g., bathymetry, bedforms), dynamic surface conditions with downwelling, subducted bubbles, mixing and turbulence at the front, and potential presence of migrating fish and internal waves propagating along the density contrast interface. Future work will seek to quantify the contribution of each of these physical mechanisms to estuarine acoustic propagation characteristics.

ACKNOWLEDGMENTS

The expertise and tireless efforts of the captain and crew of the R/V Oceanus (OSU), NPS Engineer Chris Miller, and UW/APL colleagues Jim Thomson, Chris Bassett, and Seth Zippel were indispensable in the collection of these data and are sincerely appreciated. Thanks to Guy Gelfenbaum

(USGS) for the use of the tripod at Station A5. Thanks also to Antonio Baptista, Charles Seaton, and Paul Turner at CMOP for modeled temperature and salinity profiles used in the acoustic modeling. This work was supported by the Office of Naval Research.

Chen, C.-T., and Millero, F. J. (**1977**). "Speed of sound in seawater at high pressures," J. Acoust. Soc. Am. **62**, 1129–1135.

Diachock, O. (**1999**). "Effects of absorbtivity due to fish on transmission loss in shallow water," J. Acoust. Soc. Am. **105**(4), 2107–2128.

Di Iorio, D., and Farmer, D. M. (**1994**). "Path-averaged turbulent dissipation measurements using high-frequency acoustical scintillation analysis," J. Acoust. Soc. Am. **96**(2), 1056–1069.

Dong, L., Wang, D., Wang, K., Li, S., Dong, S., Zhao, X., Akamatsu, T., and Kimura, S. (**2011**). "Passive acoustic survey of Yangtze finless porpoises using a cargo ship as a moving platform," J. Acoust. Soc. Am. **130**(4), 2285–2292.

Dyer, Keith (**1998**). *Estuaries: A Physical Introduction* (Wiley, New York), Chap. 1, pp. 5–25.

Elias, E. P. L., Gelfenbaum, G., and Van der Westhuysen, A. J. (**2012**). "Validation of a coupled wave-flow model in a high-energy setting: The mouth of the Columbia River," J. Geophys. Res. **117**, C09011, doi:10.1029/2012JC008105.

Etter, Paul C. (**2003**). *Underwater Acoustic Modeling and Simulation* (Spon Press, London), Chap. 4.

Fillinger, L., Sutin, A., and Sedunov, A. (**2011**). "Acoustic ship signature measurements by cross-correlation method," J. Acoust. Soc. Am. **129**(2), 774–778.

Gelfenbaum, G. (**1983**). "Suspended-sediment response to semidiumal and fortnightly tidal variations in a mesotidal estuary: Columbia River, USA," Marine Geol. **52**, 39–57.

Gelfenbaum, G., Elias, E., Stevens, A., MacMahan, J., Reniers, A., and Sherwood, C. (**2014**). "Impacts of large-scale morphology and bedforms on inlet dynamics: Mouth of the Columbia River, USA," in *Proceedings of the 17th Physics of Estuaries and Coastal Seas (PECS) Conference*, Porto de Galinhas, Pernambuco, Brazil, 19–24 October.

Geyer, Rocky (**2014**). (personal communication).

Haviland-Howell, G., Frankel, A. S., Powell, C. M., Bocconcelli, A., Herman, R. L., and Sayigh, L. S. (**2007**). "Recreational boating traffic: A chronic source of anthropogenic noise in the Wilmington, North Carolina Intracoastal Waterway," J. Acoust. Soc. Am. **122**(1), 151–160.

Jay, D. A., and Smith, J. D. (**1990**). "Circulation, density distribution and spring-neap transitions in the Columbia River estuary," Prog. Oceanogr. **25**, 81–112.

Lavery, A. C., Geyer, W. R., and Scully, M. E. (**2013**). "Broadband acoustic quantification of stratified turbulence," J. Acoust. Soc. Am. **134**(1), 40–54.

McConnell, S. O., Schilt, M. P., and Dworski, J. G. (**1992**). "Ambient noise measurements from 100 Hz to 80 kHz in an Alaskan fjord," J. Acoust. Soc. Am. **91**(4), 1990–2003.

McNeil, C. L., Shcherbina, A., Litchendorf, T., Sanford, T. B., Martin, D., Bapista, A. M., Lopez, J., and Crump, B. (**2012**). "Observations of the Columbia River salt wedge and estuarine turbidity maximum using AUVs," Abstract OS11G-07, presented at the *2012 Fall Meeting, AGU*, San Francisco, CA, 3–7 December.

Neal, V. T. (**1972**). "Physical aspects of the Columbia River and its estuary," in *The Columbia River Estuary and Adjacent Ocean Waters*, edited by A. T. Pruter and D. L. Alverson (University of Washington Press, Seattle, WA), pp. 19–40.

Poikonen, A. A. (**2010**). "High-frequency wind-driven ambient noise in shallow brackish water: Measurements and spectra," J. Acoust. Soc. Am. **128**(5), EL242–EL247.

Porter, M. B., and Bucker, H. P. (**1987**). "Gaussian beam tracing for computing ocean acoustic fields," J. Acoust. Soc. Am. **82**(4), 1349–1359.

Radhakrishnan, S. (**2009**). "Acoustic propagation in the Hudson River Estuary: Analysis of experimental measurements and numerical modeling results," Ph.D. dissertation, Stevens Institute of Technology, Publication Number 3351563.

Reeder, D. Benjamin (**2013**). "Acoustical characterization of the estuarine salt wedge," POMA **19**, 005004.

Reeder, D. Benjamin, and Stanton, T. K. (**2004**). "Acoustic scattering by axisymmetric finite-length bodies: An extension of a 2-dimensional conformal mapping method," J. Acoust. Soc. Am. **116**(2), 729–746.

Roh, H.-S., Sutin, A., and Bunin, B. (**2008**). "Determination of acoustic attenuation in the Hudson River Estuary by means of ship noise observations," J. Acoust. Soc. Am. **123**(6), EL139–EL143.

Sherwood, C. R., and Creager, J. S. (**1990**). "Sedimentary geology of the Columbia River estuary," Prog. Oceanogr. **25**, 15–79.

Sherwood, C. R., Jay, D. A., Harvey, R. B., Hamilton, P., and Simenstad, C. A. (**1990**). "Historical changes in the Columbia River estuary," Prog. Oceanogr. **25**, 299–352.

Stolkin, R., Sutin, A., Radhakrishnan, S., Bruno, M., Fullerton, B., Ekimov, A., and Raftery, M. (**2006**). "Feature based passive acoustic detection of underwater threats," in *Photonics for Port and Harbor Security II*, Proceedings of SPIE, edited by M. DeWeert, T. T. Saito, and H. L. Guthmuller, Vol. 6204, p. 620408.

Thomson, J., Horner-Devine, A. R., Zippel, S., Rusch, C., and Geyer, W. (**2014**). "Wave breaking turbulence at the offshore front of the Columbia River Plume," Geophys. Res. Lett. **41**, 8987–8993, doi:10.1002/2014GL062274.

van Walree, P. A., Neasham, J. A., and Schrijver, M. C. (**2007**). "Coherent acoustic communication in a tidal estuary with busy shipping traffic," J. Acoust. Soc. Am. **122**(6), 3495–3506.

Vracar, M. S., and Miomir, M. (**2011**). "Ambient noise in large rivers (L)," J. Acoust. Soc. Am. **130**(4), 1787–1791.

Wysocki, L. E., Amoser, S., and Ladich, F. (**2007**). "Diversity of ambient noise in European freshwater habitats: Noise levels, spectral profiles, and impact on fishes," J. Acoust. Soc. Am. **121**(5), 2559–2566.

Xie, Y. (**2000**). "A range-dependent echo-association algorithm and its application in split-beam sonar tracking of migratory salmon in the Fraser River watershed," J. Ocean Eng. **25**(3), 387–398.

Zhou, J.-X., Zhang, X.-Z., and Knobles, D. P. (**2009**). "Low-frequency geoacoustic model for the effective properties of sandy seabottoms," J. Acoust. Soc. Am. **125**(5), 2847–2866.

Zhu, X.-H., Zhang, C., Wu, Q., Fan, X., and Li, Bo (**2010**). "Acoustic measurement of tidal bores in the Qiantang River, China," in *Proceedings of the 3rd International Congress on Image and Signal Processing (CISP)*, pp. 3839–3843.